JOURNAL OF NEUROTRAUMA
Volume 24, Number 5, 2007

Pp. 812–822
DOI: 10.1089/neu.2006.0169

Mechanical Heterogeneity of the Rat Hippocampus Measured by Atomic Force Microscope Indentation

BENJAMIN S. ELKIN, EVREN U. AZELOGLU, KEVIN D. COSTA, and BARCLAY MORRISON III

ABSTRACT

Knowledge of brain tissue mechanical properties may be critical for formulating hypotheses about traumatic brain injury (TBI) mechanisms and for accurate TBI simulations. To determine the local mechanical properties of anatomical subregions within the rat hippocampus, the atomic force microscope (AFM) was adapted for use on living brain tissue. The AFM provided advantages over alternative methods for measuring local mechanical properties of brain because of its high spatial resolution, high sensitivity, and ability to measure live samples under physiologic conditions. From AFM indentations, a mean pointwise or depth-dependent apparent elastic modulus, $\hat{E}$, was determined for the following hippocampal subregions: CA1 pyramidal cell layer (CA1P) and stratum radiatum (CA1SR), CA3 pyramidal cell layer (CA3P) and stratum radiatum (CA3SR), and the dentate gyrus (DG). For all regions, $\hat{E}$ was indentation-depth-dependent, reflecting the nonlinearity of brain tissue. At an indentation depth of 3 μm, $\hat{E}$ was 234 ± 152 Pa for CA3P, 308 ± 184 Pa for CA3SR, 137 ± 97 Pa for CA1P, 169 ± 52 Pa for CA1SR, and 201 ± 133 Pa for DG (mean ± SD). Our results demonstrate for the first time that the hippocampus is mechanically heterogeneous. Based on our findings, we discuss hypotheses accounting for experimentally observed patterns of hippocampal cell death, which can be tested with biofidelic finite element models of TBI.

Key words: brain tissue; elasticity; heterogeneity; hippocampus; mechanical properties

INTRODUCTION

TRAUMATIC BRAIN INJURY (TBI) is a leading cause of death and disability worldwide (Tagliaferri et al., 2006; Thurman et al., 1999). The large societal costs of TBI motivate the study of brain injury biomechanics to improve protection systems (e.g., vehicular restraints, helmets) (Nirula et al., 2004), improve safety standards through development of more appropriate tolerance criteria (Cater et al., 2006; Zhang et al., 2004), and to further our understanding of the biological mechanism(s) of injury which could lead to improved treatments for the head injured patient (Zhang et al., 2005).

In vivo models of TBI, such as fluid percussion injury (FPI) or controlled cortical impact (CCI), are in widespread use (Morales et al., 2005) and demonstrate a distinct pattern of cell death within the hippocampus which has not been explained. After experimental TBI, greater cell death is localized to the CA3 region of the pyramidal cell layer as compared to the CA1 region (Anderson

Department of Biomedical Engineering, Columbia University, New York, New York.

et al., 2005; Colicos et al., 1996; Grady et al., 2003; Hicks et al., 1996; Kim et al., 2001; McCullers et al., 2002; Scheff et al., 2005). There are three hypotheses that may, alone or together, be capable of explaining this pattern: (1) the pyramidal cells of CA1 are less susceptible to injury than those of CA3 given the same mechanical stimulus—i.e., that CA1 and CA3 possess different intrinsic tolerance criteria; (2) differences in mechanical properties between the two regions may result in heterogeneous strain fields (and hence cell death) *in vivo* during injury; and (3) the injury loading conditions contribute to producing heterogeneous strain distributions that correlate with the observed pattern of cell death. Previously, we tested the first hypothesis using an *in vitro* model of TBI that induces tissue deformation independent of tissue mechanical properties. Organotypic slice cultures of the hippocampus were subjected to precisely controlled stretch (equibiaxial strain ranging from 0 to 0.5, and strain rate ranging from 0 to 50 sec^{-1}). We found that both regions exhibited the same time course and magnitude of cell death following injury (Cater et al., 2006), which suggests that CA1 and CA3 possess similar intrinsic tolerance criteria (i.e., that CA3 is not intrinsically more vulnerable to injury).

In light of our previous findings, we set out to test the basis for the second hypothesis: whether the two hippocampal regions possess different mechanical or structural properties, which could potentially result in regional differences of strain induced by mechanical loads imposed during TBI *in vivo*. The experimentally observed pattern of cell death might then be correlated with a heterogeneous pattern of induced strain which could be predicted by sophisticated computational models incorporating heterogeneous mechanical properties within the hippocampus. These computational models would also be capable of testing the third hypothesis by assuming homogeneous mechanical properties. In the current study, we measured the structural stiffness of distinct morphologic regions of the hippocampus to characterize this spatial distribution of mechanical properties.

Measuring the mechanical properties of brain tissue is challenging due to its morphologic heterogeneity, low modulus of elasticity, and dependence on its physiologic state (i.e., living vs. dead, time postmortem, environment) (Fountoulakis et al., 2001; Gefen et al., 2004; Metz et al., 1970). Previous studies have endeavored to characterize the mechanical properties of brain tissue in various species (Donnelly et al., 1997; Nicolle et al., 2005). While some studies have shown mechanical differences between gross anatomic regions of the brain, such as white matter versus grey matter (Prange et al., 2002), mechanical properties within these regions at finer spatial scales corresponding to anatomically distinct structures have not been examined.

Current methodologies for measuring the mechanical properties of brain tissue (i.e., unconfined compression, parallel plate shear, and macroindentation) require large, homogeneous samples relative to anatomical structures. They are incapable of measuring small enough samples to resolve the heterogeneity within the gray or white matter regions. In addition, while the majority of *in vivo* TBI models are in the rat (Morales et al., 2005), there is a paucity of data on the mechanical properties of rat brain tissue. This lack of rat-specific data may be due to the incompatibility of previous methodologies for testing small samples; the adult rat brain is quite small ($\sim$20 mm $\times$ 15 mm $\times$ 10 mm) (Paxinos et al., 1998). Finally, most studies have been performed on non-living tissue whose mechanical properties may have already begun to change (Fountoulakis et al., 2001) and may not correlate to those *in vivo* (Gefen et al., 2004).

The atomic force microscope (AFM) has emerged as a viable option for measuring the mechanical properties of small, live, biological specimens (Rotsch et al., 2000; Stolz et al., 2004; Takai et al., 2005). We have found that AFM indentation is an appropriate method for measuring the material properties of rat brain tissue due to its high sensitivity, high spatial resolution, and compatibility with living samples. In this study, the AFM was used to measure the local mechanical properties within the rat hippocampus. The spatial resolution of the AFM allowed us to evaluate the mechanical heterogeneity between distinct morphologic regions within the hippocampus, such as the CA1 and CA3 pyramidal cell layers, CA1 and CA3 stratum radiatum, and the dentate gyrus. Measurements with the AFM were performed at 37°C in aqueous, osmotically, and pH-balanced medium to maintain the tissue in a physiologic state.

METHODS

Hippocampal Slice Preparation

All animal procedures were approved by the Columbia University Institutional Animal Care and Use Committee (IACUC). Hippocampi were removed from 8–10-day-old Sprague-Dawley rats. Hippocampi for AFM studies were sliced at a thickness of 400 μm, whereas hippocampi for bulk material studies were sliced at a thickness of 1 mm, both using a McIlwain tissue chopper (Harvard Apparatus, Holliston, MA). Slices were separated in ice-cold Geys salt solution (Sigma, St. Louis, MO) supplemented with 4.5 mg/mL D-glucose using sterile blunt plastic spatulas. Slices were then plated on nonporous silicone membranes (Specialty Manufacturing,

Saginaw, MI) coated with laminin and poly-D-lysine, bathed in Neurobasal medium (Invitrogen; supplemented with 1 mM L-glutamine, B27, and 4.5 mg/mL D-glucose), and placed on a rocker in an incubator at 37°C to allow for adhesion to the silicone substrate (Cater et al., 2006a,b; Morrison et al., 2006).

Scanning Electron Microscopy

Tissue slices were rinsed in ice cold PBS and fixed for 1 h in 4% formaldehyde. Slices were dehydrated in a series of increasing concentrations of ethanol to 100%. Slices were then dried using a critical point drier (Electron Microscopy Sciences, Hatfield, PA) and sputter-coated with gold. Images were acquired using a Hitachi 4700 scanning electron microscope.

Nissl Staining

Tissue slices were rinsed in ice cold PBS and fixed for 1 h in 4% formaldehyde. Slices were then dehydrated in a series of increasing concentrations of ethanol to 100% and then xylene. Slices were embedded in paraffin and sectioned at a thickness of 10 μm on a microtome. Sections were then mounted on slides, rehydrated, stained in 0.02% thionin, dehydrated, and coverslipped with permount (Sigma).

Bulk Material Property Testing

Unconfined compression tests were performed on 1 mm thick hippocampal slices using a two-platen device mounted on an inverted light microscope. The platens were displacement-controlled using a custom written LabView (National Instruments, Austin, TX) program capable of controlling compression ramp speed and magnitude. Sample surface area was calculated prior to the compression test using ImageJ (NIH, Bethesda, MD). Equilibrium stress was measured at the end of 25% compression tests using an axial force transducer (Transducer Techniques, Temecula, CA) from which a structural modulus for the entire slice was calculated. The duration of compression tests was 360 sec at which point equilibrium was assumed. An equilibrium elastic modulus, E, was calculated as follows:

$$E = \frac{F/A}{\varepsilon}$$

where F was equilibrium force, A was cross-sectional area, and ε (=0.25) was axial engineering strain. Equilibrium force, F, was calculated by taking the average force over the final 60 sec of the test.

Atomic Force Microscopy

An atomic force microscope (AFM; Bioscope, Veeco, Santa Barbara, CA) mounted on an inverted light microscope (IX-81; Olympus, Melville, NY) was used to measure material properties within local regions of the hippocampus. The cantilever probe used for all indentations had a nominal spring constant, k, of 0.12 N/m with a 25-μm polystyrene sphere attached to the tip (Novascan, Ames, IA). Sphere diameter for the probe tip was verified under a calibrated light microscope.

Hippocampal slices were retrieved after 2–4 h in the incubator, sufficient time for them to adhere to the silicone substrate, and the medium was changed to a CO_2-independent medium (Invitrogen) supplemented with 4.5 mg/mL D-glucose. Slices equilibrated for 10 min on the heated AFM stage (maintained at 37°C) before measurements were performed. The cantilever probe was mounted on a fluid cell with a modified moisture trap cuff to ensure that media would not evaporate during the measurement procedure. All indentations were performed at 0.5 Hz with an 11.55-μm ramp resulting in indenter velocities of 11.55 μm/sec.

Two sets of indentation experiments were performed. In the first study, slices were indented along a track which traverses the major anatomically distinct hippocampal regions beginning with the pyramidal cell body layer from CA1 to CA3 and CA4, then crossing the dentate gyrus, and ending in the stratum oriens of CA1 ($n = 3$ slices). Overlapping measurements in the pyramidal cell layer of CA1 verified that slice stiffness was not altered during the course of the experiment. For this study, indentations arranged in 3×3 arrays with 6-μm spacing were performed at each measurement location along the track. A spacing of 6 μm was chosen so that each indentation would not interfere with the preceding and following indentation. In a second set of studies, distinct anatomical regions (in a randomized order) were indented in locations within a 6×6 array with 6-μm spacing. Regions investigated included the CA1 and CA3 pyramidal cell layers, the CA1 and CA3 stratum radiatum, and the dentate gyrus ($n = 7$ slices).

Data Analysis

Contact point was identified from raw deflection versus displacement data (force curves) for each indentation using the following algorithm implemented in MATLAB: (1) Force curves exhibiting positive pre-contact slope or too little pre- or post-contact data were eliminated from the analysis by visual inspection. (2) Deflection versus displacement data was fit to an 8th order polynomial (sufficient to eliminate noise from the data for implementation of step 3); the first and last 100 data points were not included in this step to ensure a high-quality fit. (3) The contact point was then identified as the first point at which the instantaneous 1st and 2nd derivates were both

greater than an empirically determined threshold (Fig. 1). This protocol was applied identically to each force curve using the same thresholds for all curves. This approach was favored over that proposed by Crick et al. (2006) due to its ability to properly identify contact points for highly nonlinear tissue and to compensate for the relative nonlinearity of precontact data (most likely due to the large z-ramp used for this study), both being stated limitations of the Crick and Yin approach. From the raw post-contact deflection data, a pointwise apparent elastic modulus ($\hat{E}$) was calculated for each indentation depth using the following equation (Costa et al., 1999; Costa, 2003):

$$\hat{E} = \frac{3(1 - \nu^2) \cdot k \cdot h}{4\sqrt{R}D^3}$$

where k was the spring constant of the cantilever probe, h was the cantilever deflection, R was the spherical radius of the probe tip, D was the indentation depth, and ν was the Poisson's ratio of brain assumed to be 0.5 (Darvish et al., 2001; Lippert et al., 2004). Assuming a smaller Poisson's ratio (e.g., 0.3 or 0.4) would increase the estimation of $\hat{E}$ by 21% and 12%, respectively. Our primary goal however was to demonstrate relative differences in $\hat{E}$ rather than absolute values. Pointwise apparent elastic moduli are reported for the first 3 μm of indentation at 100-nm intervals. For the stiffer regions of the hippocampus, deeper indentation depths were outside the range of the AFM instrumentation in its current configuration.

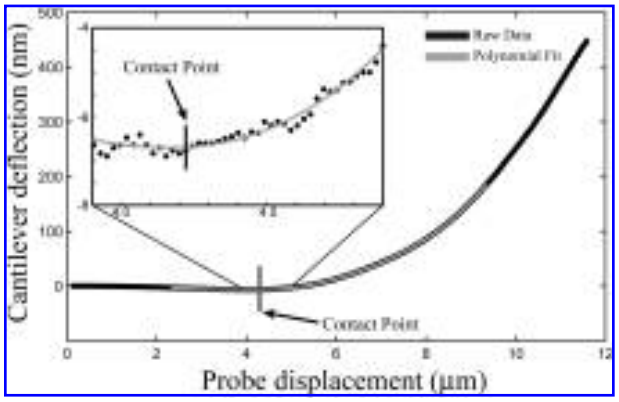

FIG. 1. Representative force curve from the CA1 pyramidal cell layer. The raw data (black) was fit to an 8th order polynomial (gray) to eliminate noise during contact point identification. The contact point (arrow) was identified as the point at which the 1st and 2nd derivative of the polynomial exceeded an empirically determined threshold (slightly greater than zero). This same threshold was applied to all force curves which produced reasonable estimates of contact point upon visual inspection. Pointwise apparent elastic modulus, $\hat{E}$, was then calculated from the raw post-contact data. (**Inset**) Magnification of force curve illustrating the smoothing effect of the polynomial fit (gray line) to the raw data (black circles).

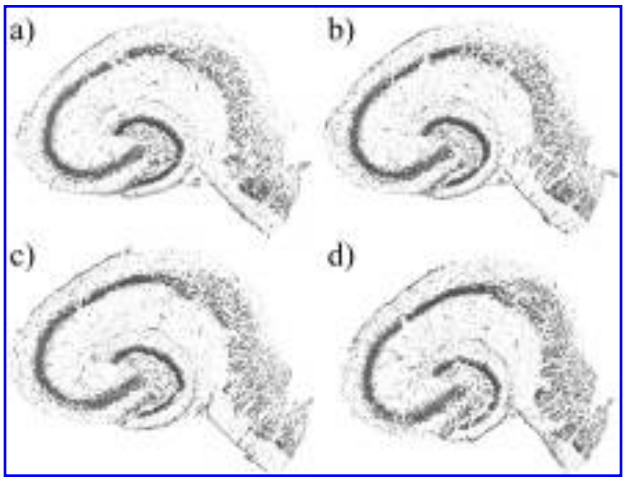

FIG. 2. Four 10-μm-thick Nissl-stained, serial sections (**a–d**) of a hippocampus used for atomic force microscope (AFM) measurements showing through thickness homogeneity. The morphology remains consistent within the vertical direction of indentation. These slices represent sections from a total of 40 μm in the vertical direction of indentation. Maximum indentation depth was 3 μm.

Statistical Analysis

The mean apparent elastic modulus at both a small and large indentation depth of 0.5 and 3 μm for each region was calculated from the force curves which met criteria listed above. Since each indentation was performed in a different location within each region of each slice, each was considered an independent measurement. Levene test for homogeneity indicated that variances were unequal ($p < 0.05$). The means were then analyzed by one-way analysis of variance (ANOVA) with a Brown Forsythe test to account for unequal variances followed by Bonferroni post-hoc tests using SPSS (SPSS Inc., Chicago, IL) to evaluate differences between regions. A p-value of <0.05 was considered statistically significant.

RESULTS

Figure 2 shows four Nissl-stained 10-μm-thick serial sections from a slice of hippocampus used for AFM. These sections illustrate the through thickness homogeneity that was assumed for each region measured. Measured nonlinearity was therefore attributable to tissue properties and not to through-thickness, tissue heterogeneities at increasing depths of indentation. Pyramidal neuronal cell bodies, which are stained darkly in Figure

2, are concentrated in the pyramidal cell layers with their processes projecting into the stratum radiatum and stratum oriens accompanied by glia and a sparse distribution of interneurons.

Figure 3a is a scanning electron micrograph of the surface of a slice used for AFM studies within the CA3 stratum radiatum. The main structural elements of the tissue form a porous mesh exhibiting many pits and valleys with diameters ranging from 2 to 8 μm. The 25-μm sphere attached to the indentation probe shown in Figure 3b was large relative to the scale of the tissue surface features. This ensured that the surface was indented evenly, that the surface texture did not affect the indentation, and that the probe did not bury itself into one of the many pits and valleys.

Measurements tracking along the cell body layer revealed a heterogeneity of stiffness between regions. The location of measurements within the slices are shown in Figure 4a. Apparent elastic moduli relative to the mean of all indentations at a 3-μm indentation depth ($n = 3$ slices) for each measurement position are shown as a color-scaled overlay on an image of an actual slice (Fig. 4b). Mechanical properties of the slice were dependent on the location within the slice and the anatomical structure being probed. Of particular interest was the transition at position 11 where the modulus increases corresponding to the morphological and anatomical transition from the CA1 pyramidal cell layer to the CA3 pyramidal cell layer.

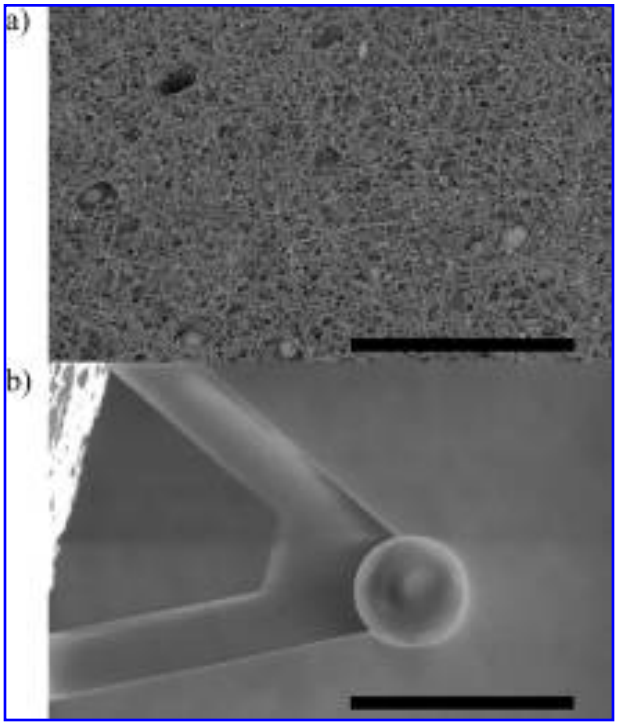

FIG. 3. (**a**) Scanning electron micrograph of the CA3 stratum radiatum depicting the surface topology that was indented by the atomic force microscope (AFM) probe. The surface was not smooth, precluding the use of a standard pyramidal AFM probe. (**b**) A large diameter (25 μm) spherical-tipped AFM probe was used for indentations to compensate for surface roughness and to ensure that cellular and tissue-level properties were measured as opposed to subcellular properties. Scale bar = 50 μm.

The purpose of the study was to compare the mechanical response of different anatomic regions within the hippocampus. Therefore, slices were tested within the morphologic regions under consideration (CA1 and CA3 pyramidal cell layers and stratum radiata, as well as, the dentate gyrus; Fig. 5a). Pointwise apparent elastic modulus, $\hat{E}$, was plotted in Figure 5b as a function of indentation depth for each anatomic region. The non-linearity of the pointwise apparent elastic modulus with respect to indentation depth reflects the brain tissue's mechanical property nonlinearity and is different for each region examined. Initially, the apparent elastic modulus decreases with increasing indentation depth but increases at depths greater than 0.5 μm. The CA3 stratum radiatum and pyramidal cell layer exhibit the most strongly depth-dependent $\hat{E}$ of all the regions.

Mean $\hat{E}$ was then analyzed for significance at two different indentation depths: 0.5 and 3 μm (Fig. 6). At an indentation depth of 0.5 μm, only the CA3 stratum radiatum was significantly stiffer than all other regions, whereas all other regions were not significantly different from each other (Fig. 6a). At an indentation depth of 3 μm, however, there was a significant difference between the CA1 (137 $\pm$ 97 Pa, mean $\pm$ SD) and CA3 (234 $\pm$ 152 Pa) pyramidal cell layers ($p < 0.05$). CA3 stratum radiatum (308 $\pm$ 184 Pa) was significantly more stiff than all other regions of the hippocampus under consideration ($p < 0.05$) including its adjacent CA3 pyramidal cell layer while the CA1 stratum radiatum (169 $\pm$ 52 Pa) was not significantly different than its adjacent CA1 pyramidal cell layer ($p = 0.1$).

To compare the results obtained above for the mechanical properties of the hippocampus to those measured using a more traditional macroscale approach, unconfined compression tests were performed on freshly dissected slices of the hippocampus. Unconfined compression tests at 25% compressive strain produced a mean elastic modulus of 662 $\pm$ 87 Pa ($n = 5$ slices). This elastic modulus was twofold larger than the stiffest region of the hippocampus as measured by the AFM (CA3SR = 308 $\pm$ 184).

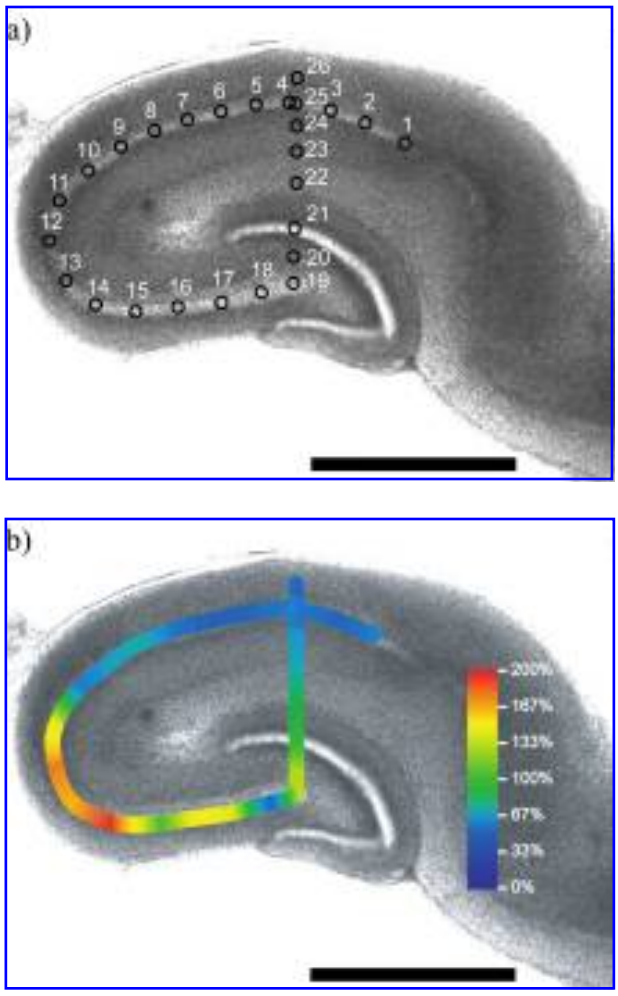

FIG. 4. (**a**) Locations of indentations performed along the pyramidal cell body layer from CA1 to CA3 then radially outward from the hilus to the stratum oriens of CA1 are depicted. (**b**) Apparent elastic modulus normalized to the mean apparent elastic modulus of all indentations is depicted by the color bar. The CA3 pyramidal cell layer was stiffer than the CA1 pyramidal cell layer. The material properties of the hippocampus were spatially heterogeneous. Scale bar = 1 mm.

DISCUSSION

Our study is the first to examine regional elastic modulus heterogeneity within an anatomic structure of the brain using the AFM. We have shown that, within the rat hippocampus, apparent elastic moduli of anatomically distinct regions are significantly different. The hypothesis that regional mechanical heterogeneities may explain, in part, experimentally observed *in vivo* differences in regional susceptibility to injury is therefore valid and worthy of further study.

Even within a single anatomical structure, heterogeneous mechanical properties exist which must now be

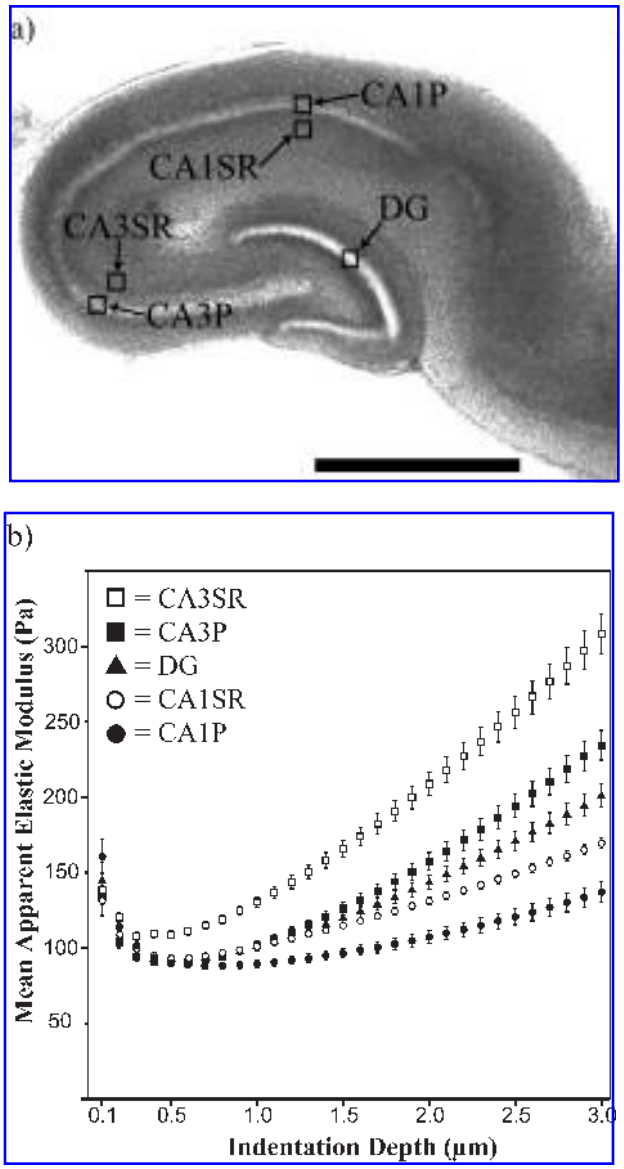

FIG. 5. (**a**) Atomic force microscope (AFM) indentations were conducted in the following regions: CA1P (CA1 pyramidal cell layer), CA3P (CA3 pyramidal cell layer), CA1SR (CA1 stratum radiatum), CA3SR (CA3 stratum radiatum), and DG (dentate gyrus). (**b**) Pointwise apparent elastic modulus is plotted as a function of indentation depth for each region measured within the hippocampus (n = 7 slices; error bars: ±SEM). Apparent elastic modulus was nonlinear with respect to indentation depth. This nonlinearity is different for each region under consideration. Scale bar = 1 mm.

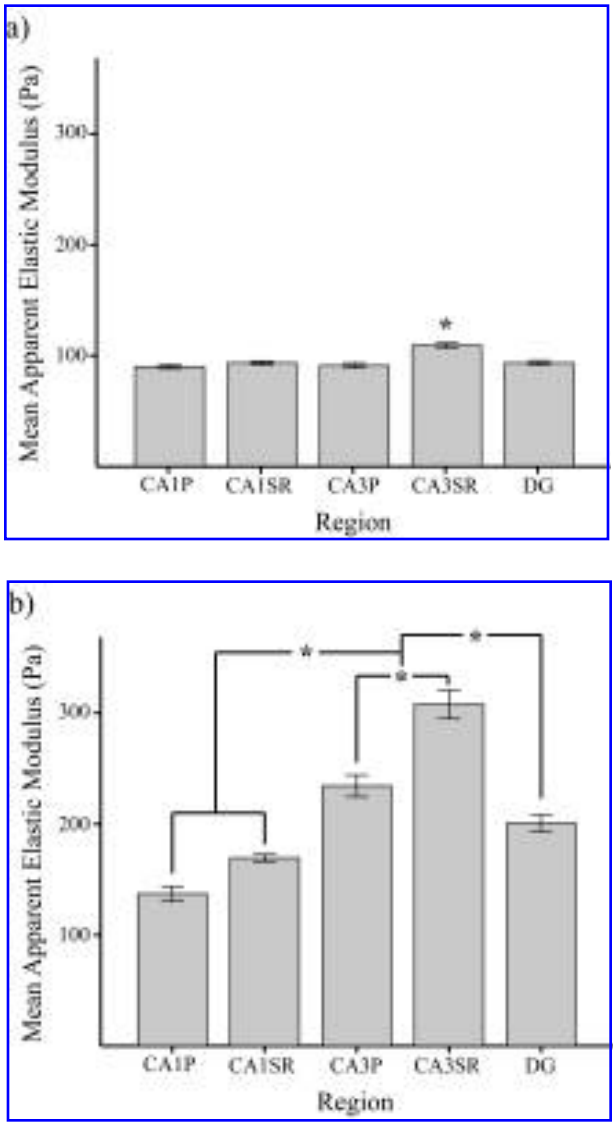

FIG. 6. Mean apparent elastic modulus at indentation depths of 0.5 μm (**a**) and 3 μm (**b**) is plotted ($n = 7$ slices; error bars: $\pm$SEM). *Significance from Bonferroni post-hoc test ($p < 0.05$). At an indentation depth of 0.5 μm, the only region that is significantly different than all others is CA3SR. At an indentation depth of 3 μm, all regions are significantly different from each other except CA1P/CA1SR and CA1SR/DG.

considered when studying TBI biomechanics. The tissue's apparent elastic properties were found to be nonlinear, exhibiting a depth-dependent stiffening of the pointwise modulus (Fig. 5b). Although similar behavior can arise from through-thickness heterogeneity of material properties (Costa et al., 1999), histological analysis of serial sections suggests the samples are relatively homogeneous along the axis of indentation. The initial decrease in modulus may be due to the settling of the probe tip within the small pits and valleys on the tissue surface. Given the estimated size of the pits and valleys (~2–8 in diameter), the probe tip should settle at an indentation depth of ~0.04–0.66 μm, which corresponds to the depths at which the modulus begins to increase. At larger depths, the CA3 stratum radiatum and pyramidal cell layer demonstrated the greatest degree of stiffening compared to the other regions tested. We also found that the CA3 pyramidal cell layer is significantly stiffer than the CA1 pyramidal cell layer at a 3-μm indentation depth (Fig. 6b). At the same indentation depth, the CA3 pyramidal cell layer is also significantly less stiff than its adjacent stratum radiatum, while the CA1 pyramidal cell layer is not significantly different from its adjacent stratum radiatum.

We hypothesized that mechanical differences between CA1 and CA3 could contribute to the regional susceptibility of the CA3 region to injury reported from *in vivo* models of TBI in the rat. We conclude that the CA3 pyramidal cell layer is significantly stiffer than the CA1 pyramidal cell layer. At first, this difference appears contrary to our hypothesis as it could lead to greater strain during TBI in the CA1 pyramidal region compared to CA3 thereby resulting in greater cell death in CA1. We offer two potential alternate interpretations. One is that the CA3 region may bear more of the load during TBI than the CA1 region resulting in large stress concentrations within CA3 which may be a contributing factor to the deleterious cellular response. This stress concentration could be considered analogous to intracranial pressure spikes often used as a predictor of tissue damage (Zhang et al., 2001). An alternative explanation is that the modulus mismatch at the interface between the CA3 pyramidal layer and the surrounding stratum radiatum, which is not as pronounced in CA1, could potentially create a region of high shear stress similar to that observed at the interface of grey and white matter reported previously in a computational model of TBI (Zhou et al., 1995). During a TBI event, this region of high shear stress could damage or shear neuronal processes exiting the CA3 pyramidal cell layer as they project into the stratum radiatum. This shear concentration could cause structural damage and/or initiate signaling cascades leading to diffuse axonal injury (DAI) (Buki et al., 2006; LaPlaca et al., 2005). In previous studies, the effect of process damage on the cell body was dependent on the proximity of that damage to the cell body (Rosenberg et al., 1997). The closer to the cell body that transection occurred, the higher the chance of cell death, suggesting that the modulus mismatch between the CA3 pyramidal cell layer and the surrounding stratum radiatum could be especially damaging. Future finite element analysis, incorporating data collected here and the hippocampal tolerance crite-

ria previously reported (Cater et al., 2006), will be required to determine if the measured differences actually do affect stress and strain distributions to a degree that could cause regional differences in susceptibility.

The increased stiffness of the CA3 pyramidal cell layer over the CA1 pyramidal cell layer may be explained by differences in the cytoskeletal composition of the pyramidal neurons in each region. Previous studies have shown that a heterogeneous distribution of cytoskeletal elements including neurofilaments (Lopez-Picon et al., 2003) and f-actin (Capani et al., 2001) exists in the hippocampus with more of both in CA3 compared to CA1. The local increase of these cytoskeletal elements could increase the CA3 regional stiffness (Costa et al., 2006). On a biochemical level, these cytoskeletal elements might also play a role in the regional susceptibility of CA3 to TBI. Neurofilament disruption following TBI could lead to plaque formation (Hamberger et al., 2003; Povlishock et al., 1997). F-actin is coupled to and can increase the conductivity of Ca^{2+}-activated K^+ channels (Huang et al., 2002) potentially contributing to excitotoxicity which is hypothesized to be an important cell death mechanism post-TBI. These cytoskeletal elements may also be involved in transducing mechanical signals in other ways that have yet to be elucidated (Maniotis et al., 1997). Further investigation of the mechanical response as well as the biochemical response of brain tissue to TBI will help to determine which of the above mechanisms are involved in the pathogenic response to TBI and may reveal injury pathways for therapeutic targeting as novel TBI treatments.

The apparent elastic moduli reported here using the AFM are calculated using the Hertz theory of contact between elastic solids. The apparent elastic modulus is considered pointwise in that it is dependent on the depth of indentation. Each distinct measurement location was indented only once to produce a non-preconditioned modulus (Gefen et al., 2004). The frequency of indentation was decreased as much as possible given the instrumentation constraints to limit viscoelastic effects but could not be decreased below 0.5 Hz due to adhesion of the probe to the tissue and subsequent contamination of the probe tip.

To ensure that tissue material properties were being probed rather than those of subcellular structures such as the nucleus or stress fibers, a large diameter (25 μm) spherical tipped AFM probe was employed (Fig. 3b). The AFM has previously been applied to the measurement of microscopic scale mechanical properties of biological specimens using spherical tipped probes with success, and the fidelity of AFM-measured mechanical properties at the microscopic scale to those measured using more traditional methods at the macroscopic scale has been evaluated previously (Dimitriadis et al., 2002; Mahaffy et al., 2000; Stolz et al., 2004). The mechanical properties measured herein were therefore considered representative of the macroscopic tissue. One limitation of scaling up the AFM to measure microscopic-scale properties is that AFM indentations are limited to depths of <10 μm. In this study, however, our primary goal was to identify heterogeneities in modulus between different anatomic subregions of the hippocampus, and an indentation depth of 3 μm was sufficient to achieve this goal.

The range of moduli reported herein at 3-μm indentation depth is slightly lower than those previously reported in the literature (Coats et al., 2006; Donnelly et al., 1997; Gefen et al., 2004; Nicolle et al., 2005; Prange et al., 2002). Values from the literature however are for species other than rat, other regions of the brain (cortex, thalamus, corona radiata), and, in certain cases, from samples that have been kept under unfavorable conditions for extended periods postmortem. This study was performed on juvenile brain tissue to accompany the data developed in our previous studies (Cater et al., 2006a, 2006b; Morrison et al., 2003, 2006). The age-dependence of mechanical properties has been reported for other brain regions generally showing an age-dependent decrease in stiffness (Gefen et al., 2003; Thibault et al., 1998), suggesting that the adult hippocampus will be more compliant than the values reported here for juvenile rats. The age dependence of hippocampal mechanical properties however is, as of yet, unknown and is an avenue that requires further study.

To compensate for the lack of readily comparable data, unconfined compression tests were performed on 1-mm-thick slices of the acute rat hippocampus. At a compressive strain of 25%, the elastic modulus was similar to the AFM-derived apparent elastic moduli but about twofold larger. This twofold difference could be due to the lower strains applied to the slice during AFM indentations. The AFM was capable of indenting the stiffer tissue regions only to a maximum of 4 μm. $\hat{E}$ did not plateau at any point before this maximum depth of indentation but continued to increase nonlinearly. Since brain tissue is nonlinear with respect to indentation depth as our AFM data shows, the higher modulus in the unconfined compression tests could be due to strain-dependent stiffening of the tissue to a degree that we were unable to replicate with the AFM for all regions. Recent studies on macroscopic properties of adult rat brain tissue reported an equilibrium modulus of the same order of magnitude reported herein (Georges et al., 2006).

The study of brain injury biomechanics and associated neurological damage suggests that one cause of TBI is tissue strain caused by an impact or sudden increase in angular or linear acceleration (Cater et al., 2006; LaPlaca

et al., 2005; Margulies et al., 1990; Meaney et al., 1995). Since *in vivo* brain tissue deformation is difficult to measure, computational modeling has been employed to predict brain deformations to better understand TBI biomechanics (Hardy et al., 1994; Zhang et al., 2001). As finite element meshes of the brain become more sophisticated with higher density meshes to incorporate local anatomic detail, the constitutive inputs to these models will require an equivalent degree of detail. Our results indicate that the AFM is capable of generating such data.

There are, however, limitations associated with the AFM indentation method employed in this study. Although brain is a viscoelastic tissue, we performed indentations at a single low speed of indentation (11.55 μm/sec) to determine an apparent pseudo-elastic modulus for the loading curve (Fung, 1993). As such, the elastic moduli reported here may be directly applicable to finite element models of neurosurgery where a static modulus could be sufficient to predict brain-shift during a surgical procedure (Miga et al., 2000a,b; Miller, 1999; Roberts et al., 1999). The AFM technique, however, can be extended to measure high-frequency viscoelastic properties of tissues (Darling et al., 2006; Mahaffy et al., 2000, 2004), which would be more applicable to computational models of TBI. In addition, our current system was not capable of performing indentations in excess of 4 μm. Larger indentations may produce measurements which correlate better with the large-strain properties of brain tissue more applicable to TBI. Our results do, however, demonstrate that different hippocampal regions posses different structural properties, and we expect these differences to persist at larger indentations. While other anatomic regions of the brain such as the brain stem are anisotropic, our AFM methods, in their current form, assumed tissue isotropy. Anisotropy may be an important determinant of injury induced deformations for certain tissues under particular loading scenarios (Arbogast et al., 1998; Nicolle et al., 2005; Prange et al., 2002).

Our data demonstrate, for the first time, the existence of heterogeneous material properties within the hippocampus. To accomplish these novel measurements, we adopted the AFM with its high spatial resolution, high sensitivity, and ability to measure living samples (Alessandrini et al., 2005; Costa et al., 2003). The heterogeneities that were discovered suggest that the increased stiffness of the CA3 stratum radiatum and pyramidal cell layer above all other measured regions of the hippocampus, as well as the modulus mismatch between them may contribute to the experimentally observed *in vivo* pattern of damage. Our data should help to formulate hypotheses about mechanisms of injury which could lead to a greater understanding of TBI and its neurological consequences.

ACKNOWLEDGMENTS

We acknowledge Shamik Chaudhuri for his assistance with figures, Kunal Bose for his assistance with the AFM, Van C. Mow for the use of the unconfined compression device, and Morakot Likhitpanichkul for her assistance with it. This work was supported in part by the Southern Consortium for Injury Biomechanics (to B.M.) and an NSF Career Award (BES 02-39138; to K.D.C.).

REFERENCES

ALESSANDRINI, A., and FACCI, P. (2005). AFM: a versatile tool in biophysics. Meas. Sci. Technol. **16,** R65–R92.

ANDERSON, K.J., MILLER, K.M., FUGACCIA, I., and SCHEFF, S.W. (2005). Regional distribution of fluoro-jade B staining in the hippocampus following traumatic brain injury. Exp. Neurol. **193,** 125–130.

ARBOGAST, K.B., and MARGULIES, S.S. (1998). Material characterization of the brainstem from oscillatory shear tests. J. Biomech. **31,** 801–807.

BUKI, A., and POVLISHOCK, J.T. (2006). All roads lead to disconnection? Traumatic axonal injury revisited. Acta Neurochir. **148,** 181–193.

CAPANI, F., ELLISMAN, M.H., and MARTONE, M.E. (2001). Filamentous actin is concentrated in specific subpopulations of neuronal and glial structures in rat central nervous system. Brain Res. **923,** 1–11.

CATER, H.L., SUNDSTROM, L.E., and MORRISON III, B. (2006a). Temporal development of hippocampal cell death is dependent on tissue strain but not strain rate. J. Biomech. **39,** 2810–2818.

CATER, H.L., GITTERMAN, D., DAVIS, S.M., BENHAM, C.D., MORRISON III, B., and SUNDSTROM, L.E. (2006b). Stretch induced injury in organotypic hippocampal slice cultures reproduces *in vivo* post-traumatic neurodegeneration: role of glutamate receptors and voltage-dependent calcium channels. J. Neurochem. **101,** 434–447.

COATS, B., and MARGULIES, S.S. (2006). Material properties of porcine parietal cortex. J. Biomech. **39,** 2521–2525.

COLICOS, M.A., DIXON, C.E., and DASH, P.K. (1996). Delayed, selective neuronal death following experimental cortical impact injury in rats: possible role in memory deficits. Brain Res. **739,** 111–119.

COSTA, K.D. (2003). Single-cell elastography: probing for disease with the atomic force microscope. Dis. Markers **19,** 139–154.

COSTA, K.D., SIM, A.J., and YIN, F.C. (2006). Non-Hertzian approach to analyzing mechanical properties of endothelial cells probed by atomic force microscopy. J. Biomech. Eng. **128,** 176–184.

COSTA, K.D., and YIN, F.C.P. (1999). Analysis of indentation: implications for measuring mechanical properties with atomic force microscopy. J. Biomech. Eng. **121,** 462–471.

CRICK, S., and YIN, F. (2006). Assessing micromechanical properties of cells with atomic force microscopy: importance of the contact point. Biomech. Modeling Mechanobiol. **6,** 199–210.

DARLING, E.M., ZAUSCHER, S., and GUILAK, F. Viscoelastic properties of zonal articular chondrocytes measured by atomic force microscopy. Osteoarthr. Cartilage **14,** 571–579.

DARVISH, K.K., and CRANDALL, J.R. (2001). Nonlinear viscoelastic effects in oscillatory shear deformation of brain tissue. Med. Eng. Phys. **23,** 633–645.

DIMITRIADIS, E.K., HORKAY, F., MARESCA, J., KACHAR, B., and CHADWICK, R.S. (2002). Determination of elastic moduli of thin layers of soft material using the atomic force microscope. Biophys. J. **82,** 2798–2810.

DONNELLY, B.R., and MEDIGE, J. (1997). Shear properties of human brain tissue. J. Biomech. Eng **119,** 423–432.

FOUNTOULAKIS, M., HARDMEIER, R., HOGER, H., and LUBEC, G. (2001). Postmortem changes in the level of brain proteins. Exp. Neurol. **167,** 86–94.

FUNG, Y.C. (1993). *Biomechanics: Mechanical Properties of Living Tissues*, 2nd ed. Springer-Verlag: New York.

GEFEN, A., and MARGULIES, S.S. (2004). Are *in vivo* and *in situ* brain tissues mechanically similar? J. Biomech. **37,** 1339–1352.

GEFEN, A., GEFEN, N., ZHU, Q.L., RAGHUPATHI, R., and MARGULIES, S.S. (2003). Age-dependent changes in material properties of the brain and braincase of the rat. J. Neurotrauma **20,** 1163–1177.

GEORGES, P.C., MILLER, W.J., MEANEY, D.F., SAWYER, E.S., and JANMEY, P.A. (2006). Matrices with compliance comparable to that of brain tissue select neuronal over glial growth in mixed cortical cultures. Biophys. J. **90,** 3012–3018.

GRADY, M.S., CHARLESTON, J.S., MARIS, D., WITGEN, B.M., and LIFSHITZ, J. (2003). Neuronal and glial cell number in the hippocampus after experimental traumatic brain injury: analysis by stereological estimation. J. Neurotrauma **20,** 929–941.

HAMBERGER, A., HUANG, Y.L., ZHU, H., et al. (2003). Redistribution of neurofilaments and accumulation of beta-amyloid protein after brain injury by rotational acceleration of the head. J. Neurotrauma **20,** 169–178.

HARDY, W.N., KHALIL, T.B., and KING, A.I. (1994). Literature-review of head-injury biomechanics. Int. J. Impact Eng. **15,** 561–586.

HICKS, R., SOARES, H., SMITH, D., and McINTOSH, T. (1996). Temporal and spatial characterization of neuronal injury following lateral fluid-percussion brain injury in the rat. Acta Neuropathol. **91,** 236–246.

HUANG, H., RAO, Y., SUN, P., and GONG, L.W. (2002). Involvement of actin cytoskeleton in modulation of Ca^{2+}-activated K^+ channels from rat hippocampal CA1 pyramidal neurons. Neurosci. Lett. **332,** 141–145.

KIM, B.T., RAGHAVENDRA, V.L., SAILOR, K.A., BOWEN, K.K., and DEMPSEY, R.J. (2001). Protective effects of glial cell line-derived neurotrophic factor on hippocampal neurons after traumatic brain injury in rats. J. Neurosurg. **95,** 674–679.

LAPLACA, M.C., CULLEN, D.K., McLOUGHLIN, J.J., and CARGILL, R.S. (2005). High rate shear strain of three-dimensional neural cell cultures: a new *in vitro* traumatic brain injury model. J. Biomech. **38,** 1093–1105.

LIPPERT, S.A., RANG, E.M., and GRIMM, M.J. (2004). The high-frequency properties of brain tissue. Biorheology **41,** 681–691.

LOPEZ-PICON, F.R., UUSI-OUKARI, M., and HOLOPAINEN, I.E. (2003). Differential expression and localization of the phosphorylated and nonphosphorylated neurofilaments during the early postnatal development of rat hippocampus. Hippocampus **13,** 767–779.

MAHAFFY, R.E., SHIH, C.K., MACKINTOSH, F.C., and KAS, J. (2000). Scanning probe-based frequency-dependent microrheology of polymer gels and biological cells. Phys. Rev. Lett. **85,** 880–883.

MAHAFFY, R.E., PARK, S., GERDE, E., KAS, J., and SHIH, C.K. (2004). Quantitative analysis of the viscoelastic properties of thin regions of fibroblasts using atomic force microscopy. Biophys. J. **86,** 1777–1793.

MANIOTIS, A.J., CHEN, C.S., and INGBER, D.E. (1997). Demonstration of mechanical connections between integrins cytoskeletal filaments, and nucleoplasm that stabilize nuclear structure. Proc. Natl. Acad. Sci. USA **94,** 849–854.

MARGULIES, S.S., THIBAULT, L.E., and GENNARELLI, T.A. (1990). Physical model simulations of brain injury in the primate. J. Biomech. **23,** 823–836.

McCULLERS, D.L., SULLIVAN, P.G., SCHEFF, S.W., and HERMAN, J.P. (2002). Mifepristone protects CA1 hippocampal neurons following traumatic brain injury in rat. Neuroscience **109,** 219–230.

MEANEY, D.F., SMITH, D.H., SHREIBER, D.I., et al. (1995). Biomechanical analysis of experimental diffuse axonal injury. J. Neurotrauma **12,** 689–694.

METZ, H., McELHANEY, J., and OMMAYA, A.K. (1970). A comparison of the elasticity of live, dead, and fixed brain tissue. J. Biomech. **3,** 453–458.

MIGA, M.I., PAULSEN, K.D., HOOPES, P.J., KENNEDY, F.E., JR., HARTOV, A., and ROBERTS, D.W. (2000a). *In vivo* quantification of a homogeneous brain deformation

model for updating preoperative images during surgery. IEEE Trans. Biomed. Eng. **47,** 266–273.

MIGA, M.I., PAULSEN, K.D., KENNEDY, F.E., HOOPES, P.J., HARTOV, A., and ROBERTS, D.W. (2000b). *In vivo* analysis of heterogeneous brain deformation computations for model-updated image guidance. Comput. Methods Biomech. Biomed. Eng. **3,** 129–146.

MILLER, K. (1999). Constitutive model of brain tissue suitable for finite element analysis of surgical procedures. J. Biomech. **32,** 531–537.

MORALES, D.M., MARKLUND, N., LEBOLD, D., et al. (2005). Experimental models of traumatic brain injury: do we really need to build a better mousetrap? Neuroscience **136,** 971–989.

MORRISON, B., III, CATER, H.L., WANG, C.C.-B., et al. (2003). A tissue level tolerance criterion for living brain developed with an in vitro model of traumatic mechanical loading. Stapp Car Crash J. **47,** 93–105.

MORRISON, B., III, CATER, H.L., BENHAM, C.D., and SUNDSTROM, L.E. (2006). An *in vitro* model of traumatic brain injury utilising two-dimensional stretch of organotypic hippocampal slice cultures. J. Neurosci. Methods **150,** 192–201.

NICOLLE, S., LOUNIS, M., WILLINGER, R., and PALIERNE, J.F. (2005). Shear linear behavior of brain tissue over a large frequency range. Biorheology **42,** 209–223.

NIRULA, R., MOCK, C.N., NATHENS, A.B., and GROSSMAN, D.C. (2004). The new car assessment program: does it predict the relative safety of vehicles in actual crashes? J. Trauma **57,** 779–786.

PAXINOS, G., and WATSON, C. (1998). *The Rat Brain in Stereotaxic Coordinates*. Academic Press: San Diego.

POVLISHOCK, J.T., MARMAROU, A., McINTOSH, T., TROJANOWSKI, J.Q., and MOROI, J. (1997). Impact acceleration injury in the rat: Evidence for focal axolemmal change and related neurofilament sidearm alteration. J. Neuropathol. Exp. Neural. **56,** 347–359.

PRANGE, M.T., and MARGULIES, S.S. (2002). Regional, directional, and age-dependent properties of the brain undergoing large deformation. J. Biomech. Eng. **124,** 244–252.

ROBERTS, D.W., MIGA, M.I., HARTOV, A., et al. (1999). Intraoperatively updated neuroimaging using brain modeling and sparse data. Neurosurgery **45,** 1199–1206.

ROSENBERG, L.J., and LUCAS, J.H. (1997). The effects of ciliary neurotrophic factor on murine spinal cord neurons subjected to dendrite transection injury. Brain Res. **775,** 209–213.

ROTSCH, C., and RADMACHER, M. (2000). Drug-induced changes of cytoskeletal structure and mechanics in fibroblasts: an atomic force microscopy study. Biophys. J. **78,** 520–535.

SCHEFF, S.W., PRICE, D.A., HICKS, R.R., BALDWIN, S.A., ROBINSON, S., and BRACKNEY, C. (2005). Synaptogenesis in the hippocampal CA1 field following traumatic brain injury. J. Neurotrauma **22,** 719–732.

STOLZ, M., RAITERI, R., DANIELS, A.U., VANLANDINGHAM, M.R., BASCHONG, W., and AEBI, U. (2004). Dynamic elastic modulus of porcine articular cartilage determined at two different levels of tissue organization by indentation-type atomic force microscopy. Biophys. J. **86,** 3269–3283.

TAGLIAFERRI, F., COMPAGNONE, C., KORSIC, M., SERVADEI, F., and KRAUS, J. (2006). A systematic review of brain injury epidemiology in Europe. Acta Neurochir. **148,** 255–268.

TAKAI, E., COSTA, K.D., SHAHEEN, A., HUNG, C.T., and GUO, X.E. (2005). Osteoblast elastic modulus measured by atomic force microscopy is substrate dependent. Ann. Biomed. Eng. **33,** 963–971.

THIBAULT, K.L., and MARGULIES, S.S. (1998). Age-dependent material properties of the porcine cerebrum: effect on pediatric inertial head injury criteria. J. Biomech. **31,** 1119–1126.

THURMAN, D.J., ALVERSON, C., DUNN, K.A., GUERRERO, J., and SNIEZEK, J.E. (1999). Traumatic brain injury in the United States: a public health perspective. J. Head Trauma Rehabil. **14,** 602–615.

ZHANG, L., YANG, K.H., and KING, A.I. (2001). Comparison of brain responses between frontal and lateral impacts by finite element modeling. J. Neurotrauma **18,** 21–30.

ZHANG, L., YANG, K.H., and KING, A.I. (2004). A proposed injury threshold for mild traumatic brain injury. J. Biomech. Eng. **126,** 226–236.

ZHANG, X., CHEN, Y., JENKINS, L.W., KOCHANEK, P.M., and CLARK, R.S. (2005). Bench-to-bedside review: Apoptosis/programmed cell death triggered by traumatic brain injury. Crit. Care **9,** 66–75.

ZHOU, C., KHALIL, T.B., and KING, A.I. (1995). A new model comparing impact responses of the homogeneous and inhomogeneous human brain. Stapp Car Crash J. **39,** 121–137.

Address reprint requests to:
Barclay Morrison III, Ph.D.
Department of Biomedical Engineering
Columbia University
351 Engineering Terrace
1210 Amsterdam Avenue MC 8904
New York, NY 10027

E-mail: bm2119@columbia.edu